Scaling of multiexciton lifetimes in semiconductor nanocrystals

V. I. Klimov, J. A. McGuire, and R. D. Schaller
Chemistry Division, Los Alamos National Laboratory, Los Alamos, New Mexico 87545, USA

V. I. Rupasov
ANTEOS, Inc., Shrewsbury, Massachusetts 01545, USA
and Landau Institute for Theoretical Physics, 117940 Moscow, Russia

(Received 14 February 2008; revised manuscript received 2 April 2008; published 23 May 2008)

Ultrafast multiexciton decay via Auger recombination is a major impediment for prospective applications of semiconductor nanocrystals (NCs) in lasing and solar cells enabled by carrier multiplication. One important unexplored aspect of Auger recombination is the scaling of multiexciton lifetimes with the number of excitons per NC. To address this question, we analyze multiexciton dynamics in PbSe and CdSe NCs. We observe that these two systems show a distinct difference in scaling of multiexciton lifetimes, which can be explained in terms of a difference in symmetries of high-order multiexcitons resulting from significant disparity in degeneracies of the lowest-energy quantized states.

DOI: 10.1103/PhysRevB.77.195324 PACS number(s): 78.67.Bf, 73.21.La, 78.47.−p

I. INTRODUCTION

Using semiconductor nanocrystals (NCs), one can produce extremely strong spatial confinement of electronic wave functions not accessible with other types of nanostructures. One consequence of this extreme confinement is a significant enhancement in carrier-carrier Coulomb interactions that lead to a number of interesting physical phenomena including large splitting of electronic states induced by electron-hole (e-h) exchange coupling,[1] high-efficiency intraband relaxation via e-h energy transfer,[2,3] and ultrafast multiexciton decay via Auger recombination.[4] In the latter process, the e-h recombination energy is not emitted as a photon but is transferred to a third carrier, promoting it to a higher-energy state either within an NC[4] or outside it[5] (the latter is known as Auger ionization). Significant interest in Auger recombination in NCs has been stimulated by studies of NC lasing[6,7] as well as a recent demonstration of high-efficiency carrier multiplication[8] (CM) (generation of multiple e-h pairs by single photons), which has been considered as a potential enabler of generation-III photovoltaics.[9] In both of these prospective applications, Auger recombination represents a dominant carrier-loss mechanism. Therefore, understanding this process and its characteristic time scales is a necessary step toward, e.g., CM-enhanced solar cells.

In bulk semiconductors, Auger recombination is inhibited by kinematic restrictions imposed by energy and translational-momentum conservation.[10] However, because of relaxation of momentum conservation, its efficiency dramatically increases in zero-dimensional NCs.[4,11,12] Current knowledge of Auger recombination in NCs is far from being complete. One well established trend is linear dependence of the two-e-h-pair state (biexciton) lifetime (τ_2) on NC volume.[4] However, properties of higher-order multiexcitons remain largely unexplored. An important open question is the scaling of Auger lifetimes, τ_N, with the number of excitons, N, per NC. Understanding this scaling would allow one to predict dynamical behaviors of higher-order multiexcitons based on relaxation properties of biexcitons that have been well characterized experimentally.

As was mentioned earlier, new insights into dynamics of high-order multiexcitons can benefit a number of prospective applications of NCs. For example, in nanoparticles with highly degenerate emitting states such as those made of lead salts, Si or Ge, optical gain requires excitation of more than two e-h pairs per NC on average, and hence, its dynamics are governed by recombination of multiexciton states with $N>2$.[13] Understanding dynamics of higher-order multiexcitons is also important for potential photochemical applications of the CM process, especially, in photocatalytic transformations that require multiple reduction and/or oxidation steps such as splitting of a water molecule, which is a four-electron, four-proton process.

In this paper, we theoretically and experimentally study multiexciton dynamics in NCs of CdSe and PbSe over a wide range of NC sizes with a goal to infer the factors that determine the dependence of τ_N on N. These two materials are characterized by a significant disparity in the degeneracy factors, g, of the lowest-energy $1S$ quantized states ($g=2$ and 8 for the $1S$ electron states in CdSe and PbSe NCs, respectively). As a result, while in PbSe NCs high-order multiexcitons with N up to 8 can be built from identical $1S$ states (symmetric multiexcitons), in CdSe NCs multiexcitons with $N>2$ necessarily involve states of both S and non-S symmetries (asymmetric multiexcitons). Our quantum-mechanical modeling of Auger recombination indicates that the difference in multiexciton compositions can have a distinct impact on τ_N scaling. In the case of symmetric multiexcitons, one may expect that the scaling is determined by the statistical factor $[S_N=N^2(N-1)/2]$, which is calculated as the total number of Auger recombination pathways. On the other hand, quantum-mechanical restrictions associated with, e.g., selection rules can result in nonstatistical scaling in the case of asymmetric multiexcitons. We experimentally show that statistical scaling can be realized in PbSe NCs of large sizes, for which the $\tau_N^{-1} \propto N^2(N-1)$ dependence is observed for the regimes of both high-intensity excitation (no CM) and single-photon excitation mediated by the CM process. The analysis of multiexciton dynamics in CdSe NCs, however, indicates that in this case, the scaling is nonstatistical, likely

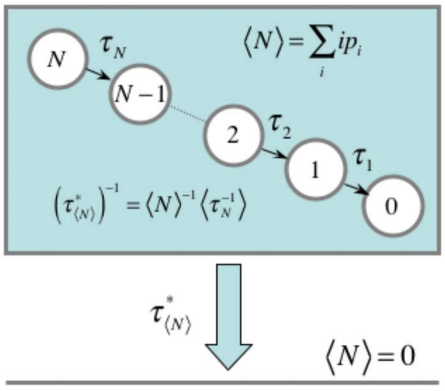

FIG. 1. (Color online) Illustration of the difference between single-NC N-exciton Auger lifetimes, τ_N, and ensemble-averaged lifetime $\tau^*_{\langle N\rangle}$.

because of the reduced probability of Auger transitions involving e-h recombination between states of different symmetries.

II. AUGER RECOMBINATION IN NANOCRYSTALS VERSUS BULK SEMICONDUCTORS

In bulk semiconductors, Auger recombination is a three-particle, cubic process[10] described by the rate equation $dn/dt=-Cn^3$ (n is the carrier density and C is the Auger constant) and the density-dependent instantaneous relaxation time, $\tau(n)=(Cn^2)^{-1}$. In the case of an NC ensemble, one can define the effective density $\langle n\rangle$ as the ratio of the NC average occupancy (the average number of e-h pairs per NC), $\langle N\rangle$, and the NC volume, V_0: $\langle n\rangle=\langle N\rangle V_0^{-1}$. Furthermore, by formally applying the bulk rate equation, one can introduce the relaxation time of the average occupancy $\tau^*_{\langle N\rangle}=-\langle N\rangle(d\langle N\rangle/dt)^{-1}=(B\langle N\rangle^2)^{-1}$ (here, $B=CV_0^{-2}$), which indicates quadratic scaling of $(\tau^*_{\langle N\rangle})^{-1}$ with $\langle N\rangle$.

In contrast to the bulk situation, in the case of NCs, an important distinction must be made between the decay time constants of the ensemble-averaged occupancy and the single-NC N-exciton state, τ_N. The latter is defined as a transition time from the N- to the $(N-1)$-exciton state (Fig. 1). Previous experimental studies indicate that Auger recombination lifetimes in CdSe and PbSe NCs are significantly shorter than radiative decay times.[4,8,14,15] Therefore, in our analysis, we assume that the decay of multiexciton states is dominated by Auger recombination (time constants τ_2, τ_3, etc.), while the single-exciton decay (time constant τ_1) is due to much slower radiative recombination.

In general, the relationship between τ_N and $\tau^*_{\langle N\rangle}$ is determined by the distribution of occupancies in an NC ensemble, which can be characterized by probabilities p_i of finding the i-exciton state in an NC sample. Temporal evolution of p_i is governed by the following set of coupled rate equations ($i=0$, 1, 2… and $\tau_0=\infty$):

$$dp_i/dt = p_{i+1}/\tau_{i+1} - p_i/\tau_i. \tag{1}$$

Multiplying each of these equations by the respective value of i and performing summation of their left- and right-hand sides, we obtain $d\langle N\rangle/dt=-\Sigma_{i=1}^{\infty}p_i\tau_i^{-1}$. This equation further yields the following expression relating the ensemble-averaged lifetime, $\tau^*_{\langle N\rangle}$, to individual multiexciton lifetimes, τ_N:

$$(\tau^*_{\langle N\rangle})^{-1} = \langle N\rangle^{-1}\sum_{i=1}^{\infty} p_i\tau_i^{-1} = \langle N\rangle^{-1}\langle\tau_N^{-1}\rangle. \tag{2}$$

In the limit of large $\langle N\rangle$, when relative variations in NC occupancies are small, Eq. (2) yields the following approximate relationship between τ_N and $\tau^*_{\langle N\rangle}$: $\tau_N=(d\langle N\rangle/dt)^{-1}|_{\langle N\rangle=N}=\tau^*_{\langle N\rangle}\langle N\rangle^{-1}|_{\langle N\rangle=N}$. This expression indicates that for the three-particle decay, for which $(\tau^*_{\langle N\rangle})^{-1}\propto\langle N\rangle^2$, τ_N^{-1} is cubic in N: $\tau_N^{-1}\propto N^3$. In the same limit ($N\gg 1$), one can express the effective NC Auger constant in terms of the N-exciton lifetime as $C_{\mathrm{NC}}=V_0^2(N^3\tau_N)^{-1}$.

It is illustrative to compare C_{NC} with respective bulk values. For example, in PbSe NCs with energy gap $E_g=0.64$ eV, $\tau_2=160$ ps (temperature $T=300$ K).[16] If we assume that the cubic scaling of τ_N^{-1} holds in the case of a small number of excitons per NC, we can calculate C_{NC} from the expression $C_{\mathrm{NC}}=V_0^2(8\tau_2)^{-1}$, which yields $C_{\mathrm{NC}}=5.6\times10^{-29}$ cm^6 s^{-1}. The bulk PbSe value of C measured in Ref. 17 is 8×10^{-28} cm^6 s^{-1}, which is greater than C_{NC}. However, such a direct comparison does not account for the difference in energy gaps of the bulk and the NC forms of PbSe. In bulk semiconductors, Auger recombination is quickly suppressed with increasing E_g. For example, in bulk PbSe, $C\propto E_g^{-11/2}\exp[-(m_t/m_l)(E_g/kT)]$,[18] where $m_{t(l)}$ is the transverse (longitudinal) carrier mass (in lead salts, electron and hole masses do not differ significantly from each other) and k is Boltzmann's constant. This expression predicts that the increase of E_g from the bulk PbSe value of 0.26 eV to the NC value of 0.64 eV should lead to a reduction of C to $\sim10^{-31}$ cm^6 s^{-1}. The latter value is much smaller (by a factor of >500) than C_{NC} measured for NCs. These considerations indicate a significant enhancement of Auger recombination in NCs compared to bulk materials.

III. QUANTUM-MECHANICAL ANALYSIS OF SCALING OF MULTIEXCITON LIFETIMES

While in the large-N limit the N-exciton lifetime is expected to be cubic in N, it is not obvious that this scaling will hold for the case when just a few e-h pairs are excited per NC. In fact, previous studies of CdSe NCs indicated a scaling that was close to quadratic.[4] To theoretically analyze the situation of small N, here, we use first-order perturbation theory.

We present the operator of the Coulomb electron-electron coupling as $H_{ee}=\int d\mathbf{r}_1 d\mathbf{r}_2\psi^\dagger(\mathbf{r}_1)\psi^\dagger(\mathbf{r}_2)U_C(|\mathbf{r}_1-\mathbf{r}_2|)\psi(\mathbf{r}_2)\psi(\mathbf{r}_1)$, where $U_C=e^2/(\kappa|\mathbf{r}_1-\mathbf{r}_2|)$ (e is the electron charge and κ is the NC dielectric permittivity) and $\psi=\Sigma_a\Psi_a(\mathbf{r})c_a+\Sigma_b\Psi_b(\mathbf{r})d_b$, in which a and b are the sets of quantum numbers for the conduction and the valence-band states, respectively, $\Psi_{a,b}$ are corresponding eigenfunctions, and $c^\dagger/d^\dagger$ (c/d) are the operators of creation (annihilation) of electrons in the conduction and/or valence band. Auger recombination can be described as scattering between two electrons in

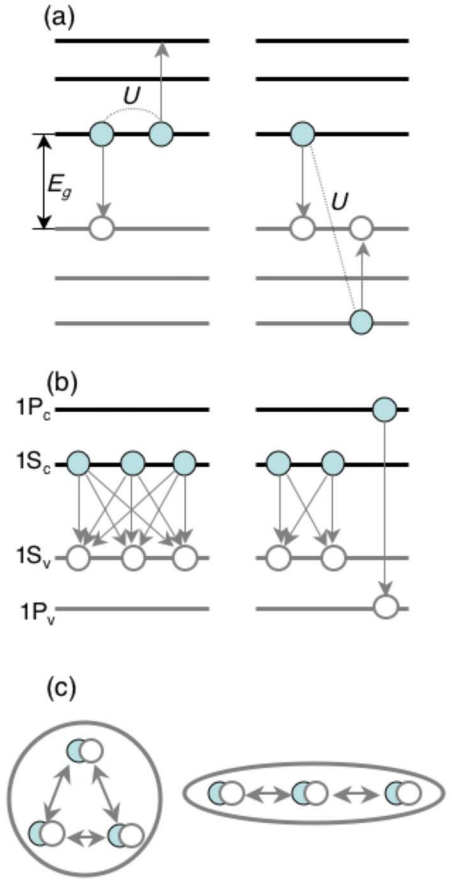

FIG. 2. (Color online) (a) Auger transitions that involve excitation of either a conduction-(left) or a valence-band (right) electron; solid and open circles correspond to electrons and holes, respectively. (b) Possible conduction-to-valence band transitions in the case of Auger recombination of a symmetric $1S1S1S$ (left) or asymmetric $1S1S1P$ (right) triexciton assuming that the S-P interband transitions are much weaker than the S-S and P-P transitions. (c) Comparison of possible energy-transfer pathways involving near-neighbor interactions during Auger recombination of a triexciton in a spherical NC (left) and an elongated quasi-1D nanorod (right).

which one is transferred from the conduction to the valence band (e-h recombination) while the other is excited within either the conduction [Fig. 2(a), left] or the valence [Fig. 2(a), right] band. The corresponding operators are, respectively, $H_{\mathrm{AR}}^{(c)}=1/2\Sigma_{a_1a_2a_3b}\Gamma_{a_2a_3}^{ba_1}d_b^\dagger c_{a_1}^\dagger c_{a_2}c_{a_3}$ and $H_{\mathrm{AR}}^{(v)}=1/2\Sigma_{a_1a_2a_3b}V_{b_3a}^{b_1b_2}d_{b_1}^\dagger d_{b_2}^\dagger d_{b_3}c_a$, where $\Gamma_{a_2a_3}^{ba_1}$ and $V_{b_3a}^{b_1b_2}$ are the antisymmetrized matrix elements of H_{ee} for the transitions shown in Fig. 2(a); they can be computed from

$$\Gamma_{a_2a_3}^{ba_1}=\int d\mathbf{r}_1d\mathbf{r}_2[\Psi_b^*(\mathbf{r}_1)\Psi_{a_1}^*(\mathbf{r}_2)-\Psi_{a_1}^*(\mathbf{r}_1)\Psi_b^*(\mathbf{r}_2)]\times U_C(|\mathbf{r}_1-\mathbf{r}_2|)\Psi_{a_2}(\mathbf{r}_2)\Psi_{a_3}(\mathbf{r}_1),$$

$$V_{b_3a}^{b_1b_2}=\int d\mathbf{r}_1d\mathbf{r}_2\Psi_{b_1}^*(\mathbf{r}_1)\Psi_{b_2}^*(\mathbf{r}_2)U_C(|\mathbf{r}_1-\mathbf{r}_2|)\times[\Psi_{b3}(\mathbf{r}_2)\Psi_a(\mathbf{r}_1)-\Psi_a(\mathbf{r}_2)\Psi_{b_3}(\mathbf{r}_1)].$$

In our calculations, we consider the Auger decay of biexciton state $|xx\rangle=c_{\alpha_2}^\dagger c_{\alpha_1}^\dagger d_{\beta_2}d_{\beta_1}|0\rangle$ into single-exciton state $|x\rangle=c_\alpha^\dagger d_\beta|0\rangle$, where $|0\rangle$ is the vacuum state. The transition amplitude for operator $H_{\mathrm{AR}}^{(c)}$ is $A_{\alpha_1\alpha_2;\beta_1\beta_2}^{(e)\alpha;\beta}=1/2\Sigma_{a_1a_2a_3b}\Gamma_{a_2a_3}^{ba_1}\langle d_\beta^\dagger c_\alpha d_b^\dagger c_{a_1}^\dagger c_{a_2}c_{a_3}c_{\alpha_2}^\dagger c_{\alpha_1}^\dagger d_{\beta_2}d_{\beta 1}\rangle$, where triangular brackets denote averaging over the NC vacuum state. To compute multiparticle correlators that enter the expression for $A_{\alpha_1\alpha_2;\beta_1\beta_2}^{(e)\alpha;\beta}$, we use the Wick theorem,[19] which allows us to replace them with a sum of products of all possible nonvanishing single-particle correlators: $\langle c_{a_2}c_{\alpha_1}^\dagger\rangle=\delta_{a_1a_2}$ and $\langle d_{b_2}^\dagger d_{b_1}\rangle=\delta_{b_1b_2}$. Using this theorem together with the condition of anticommutation of operators c and d, we can simplify the expression for the transition amplitude to $A_{\alpha_1\alpha_2;\beta_1\beta_2}^{(e)\alpha;\beta}=\Gamma_{\alpha_1\alpha_2}^{\beta_1\alpha}\delta_{\beta\beta_2}-\Gamma_{\alpha_1\alpha_2}^{\beta_2\alpha}\delta_{\beta\beta_1}$. Similarly, we can obtain the following expression for the amplitude of operator $H_{\mathrm{AR}}^{(v)}$: $A_{\alpha_1\alpha_2;\beta_1\beta_2}^{(h)\alpha;\beta}=V_{\beta\alpha_1}^{\beta_1\beta_2}\delta_{\alpha\alpha_2}-V_{\beta\alpha_2}^{\beta_1\beta_2}\delta_{\alpha\alpha_1}$. Finally, using first-order perturbation theory, we obtain the following expression for the biexciton recombination rate:

$$W_2=\frac{2\pi}{\hbar}\Bigg\{\sum_\alpha[|\Gamma_{\alpha_1\alpha_2}^{\beta_1\alpha}|^2\delta(E_{\alpha_1}+E_{\alpha_2}+E_{\beta_1}-E_\alpha)+|\Gamma_{\alpha_1\alpha_2}^{\beta_2\alpha}|^2\delta(E_{\alpha_1}+E_{\alpha_2}+E_{\beta_2}-E_\alpha)]+\sum_\beta[|V_{\beta\alpha_1}^{\beta_1\beta_2}|^2\delta(E_{\alpha_1}+E_{\beta_1}+E_{\beta_2}-E_\beta)+|V_{\beta\alpha_2}^{\beta_1\beta_2}|^2\delta(E_{\alpha_2}+E_{\beta_1}+E_{\beta_2}-E_\beta)]\Bigg\}.$$

It simplifies to $W_2=2(2\pi/\hbar)(|\Gamma|^2g_e+|V|^2g_h)$ if all of the carriers of the initial biexciton state occupy the same lowest-energy conduction ($1S_c$) or valence-band ($1S_v$) levels ($1S1S$ biexciton); here, $\Gamma=\Gamma_{1S_c1S_c}^{1S_v\alpha}$, $V=V_{\beta 1S_c}^{1S_v1S_v}$, and g_e (g_h) are the numbers of excited electron (hole) states that satisfy conservation of energy, parity, total angular momentum, and the projection thereof. The latter expression can be further generalized for the case of recombination of the N-exciton built from identical $1S$ states: $W_N=S_N(2\pi/\hbar)(|\Gamma|^2g_e+|V|^2g_h)$, where $S_N=N^2(N-1)/2$ is the statistical factor proportional to the product of the number of all possible conduction-to-valence band transitions [given by N^2; Fig. 2(b), left] and the number of carriers [e.g., electrons in the process in Fig. 2(b), left] that can accept the energy released in the individual interband transition [given by $(N-1)$]. The factor of 2 in the denominator for S_N is to avoid double counting of events, in which either one or the other electron of the interacting pair is excited up in energy; such events are already accounted for in the matrix elements Γ and V. The scaling of multiexciton lifetimes in the "statistical" case is simply determined by S_N, i.e., $\tau_N^{-1}\propto N^2(N-1)$.

Experimentally, the scaling of Auger lifetimes has often been inferred from the ratio of the triexciton and biexciton time constants.[4] In the case of statistical scaling, $\tau_2/\tau_3=4.5$. However, a different scaling might be expected if the $1S$ state can only accommodate two electrons (as, e.g., the $1S$ electron state in CdSe NCs), and hence, the triexciton, in addition to S-type carriers, also contains carriers in states of other symmetries (asymmetric triexciton). In this case, the

τ_2/τ_3 ratio becomes dependent upon the relationship between matrix elements for specific Auger transitions and, therefore, *cannot* be calculated on the basis of statistical considerations alone. One likely trend in this situation is a decrease in the decay rate of the asymmetric triexciton compared to that of the symmetric one because of the reduced probability of interband transitions between states of different symmetries. For example, if we assume that both the electron and the hole of the third exciton occupy the first-excited $1P$ state [the $1S1S1P$ triexciton; Fig. 2(b), right] and further neglect the S-P interband transitions, we obtain that τ_2/τ_3 is 2.5. This value is significantly smaller than that for statistical scaling and instead is closer to one expected for quadratic scaling ($\tau_2/\tau_3=2.25$). The general expression describing the τ_N scaling for the mixed S/P multiexcitons with $N\leq 8$ is $\tau_N^{-1}\propto[4+(N-2)^2](N-1)$ (computed neglecting S-P recombination).

In addition to quantum-mechanical restrictions, geometrical constraints can also result in deviations from statistical scaling. To illustrate this effect, we consider the situation when the Coulomb e-h interaction energy is greater than the confinement energy, and hence, electronic excitations can be described in terms of Coulombically bound e-h pairs or "true" excitons (note that in the NC literature, as in this paper, the term "exciton" is often used in a broader context and also applied to nominally unbounded e-h pairs confined not by the Coulombic potential but by the rigid boundary of the NC). Coulombically bound excitonic states are realized in, e.g., CuCl NCs[20] characterized by strong e-h attraction and elongated, quasi-one-dimensional (1D) CdSe NCs (nanorods).[21] Auger recombination in a true excitonic system is a two-particle, bimolecular process,[21] in which the energy released during recombination of one exciton is transferred to the other. In this case, the ensemble-averaged multiexciton lifetime $\tau^*_{\langle N\rangle}$ scales as $\langle N\rangle^{-1}$, while single-NC multiexciton time constants exhibit the N^{-2} scaling in the limit of large occupancies. In the small-N regime, statistical considerations predict that τ_N^{-1} is proportional to $N(N-1)$, which results in a ratio of 3 for the biexciton and the triexciton lifetimes. However, experimental studies of elongated quasi-1D NCs (quantum rods)[21] and 1D carbon nanotubes[22] indicated a τ_2/τ_3 ratio that was close to 1.5. These results point toward scaling that is slower than statistical.

One factor that could contribute to reduced scaling in 1D systems is the "chain" arrangement of interacting excitons as illustrated in Fig. 2(c) for the case of a triexciton. In a spherical NC, any of the recombining excitons that comprise a triexciton can transfer its energy to two remaining excitons with identical probabilities. On the other hand, in the case of an elongated particle, the probability of energy transfer is dependent upon the location of a particular exciton. For example, the exciton at the end of the chain will interact more strongly with its immediate neighbor than with a remote exciton on the other end of the chain. Taking into account only near-neighbor interactions, we can obtain that the τ_2/τ_3 ratio becomes 2, which is reduced compared to the statistical value. Further reduction in this ratio can result from quantum-mechanical restrictions as discussed above.

IV. SCALING OF AUGER LIFETIMES IN CADMIUN SELENIDE NANOCRYSTALS

A. Biexciton and triexciton lifetimes

An early attempt to experimentally determine the scaling of τ_N lifetimes in CdSe NCs was made in Ref. 4 where multiexciton dynamics were studied by monitoring carrier-induced bleaching of the lowest-energy $1S$ absorption feature in a femtosecond transient absorption (TA) configuration. Although pure state filling of the $1S$ state should not permit detection of dynamics of states with $N>2$, experimental data showed sensitivity to higher exciton multiplicities[4] (see next subsection), likely through effects such as Coulomb exciton-exciton interactions[23] and photoinduced absorption (PA) due to carriers trapped at NC interfaces.[24] Therefore, it was possible to extract higher-order multiexciton dynamics from the $1S$ decay using a simple "subtractive" procedure.[4]

In Fig. 3(a), we show the NC-size dependence of τ_2 (solid circles) and τ_3 (open circles) from Ref. 4 ($T=300$ K). In the present work, we have performed additional TA measurements of these lifetimes by monitoring both the lowest-energy $1S$ bleach and the higher-energy $1P$ feature. Since the major contribution to the $1P$ bleach comes from filling of the $1P$ electron state,[23] its dynamics presumably provide a more direct measure of the SSP triexciton lifetime than the $1S$ dynamics. These data are plotted in Fig. 3(a) by solid (τ_2) and open (τ_3) diamonds. In the same plot, we also show lifetimes from Refs. 25 [solid (τ_2) and open (τ_3) triangles] and 26 [solid squares (τ_2)] measured via time-resolved photoluminescence. All of these data sets obtained by different methods are consistent with each other and allow for analysis of the τ_2 and τ_3 constants over a wide range of NC radii (R).

The fit of the data for τ_2 indicates that the biexciton lifetime closely follows an R^3 dependence ($\tau_2\propto R^m; m=3.1\pm 0.4$), as was previously observed for different NC systems.[4,8,25–28] The τ_3 time constant shows a slower growth with R than τ_2. The best fit to $\tau_3\propto R^m$ indicates $m=2.6\pm 0.6$. The difference in τ_2 and τ_3 size dependences is suggestive of a size-dependent τ_N scaling.

In Fig. 3(b), we show the τ_2/τ_3 ratios for three samples (solid diamonds), for which we simultaneously measured the biexciton and the triexciton lifetimes. These data indicate that τ_2/τ_3 changes from $\sim$2.3 for $R=1.45$ nm to $\sim$3.4 for $R=4.2$ nm. For smaller sizes, the τ_2/τ_3 ratio is close to the values expected for either quantum-mechanical (2.5) or quadratic (2.25) scalings. On the other hand, for NCs of larger sizes, it approaches the cubic-scaling value (3.375) expected in the large-N limit. A similar trend, namely, the increase in the τ_2/τ_3 ratio with NC size, was observed in previous studies of CdSe NCs [open circles and solid triangles in Fig. 3(b); calculated based on data from Refs. 4 and 25, respectively].

While the τ_2/τ_3 ratios provide useful initial insight into τ_N scaling, a clearer distinction between different scaling laws can be made by analyzing higher-order multiexciton lifetimes. In Fig. 4, we compare τ_N constants for quadratic (open circles), cubic (open squares), and statistical (solid triangles) scalings calculated for the same biexciton lifetime of 130 ps. These data show that the difference between triexciton life-

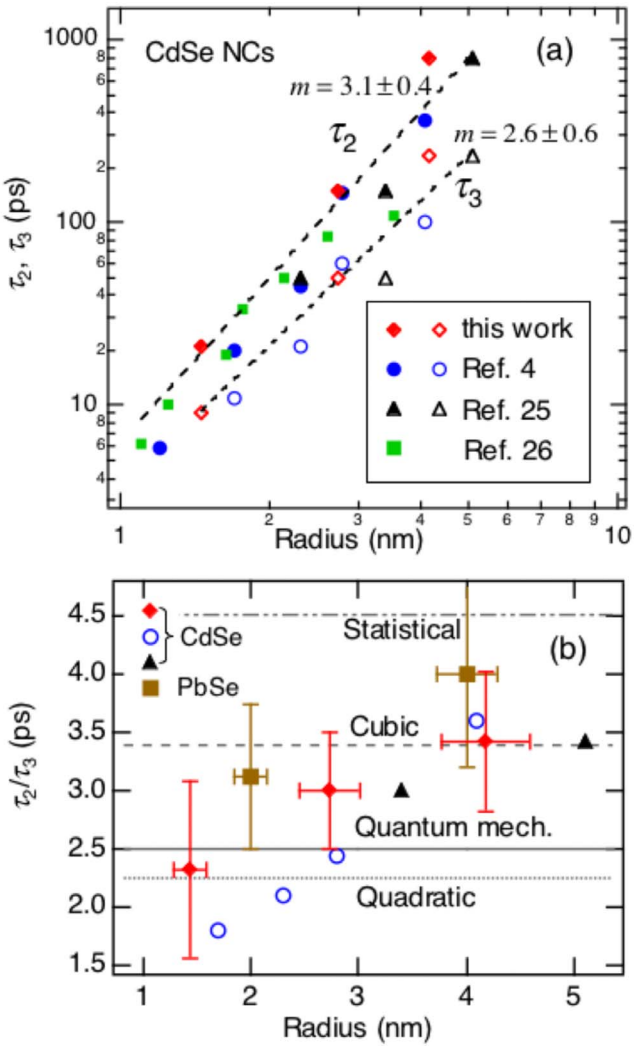

FIG. 3. (Color online) (a) The NC-size dependence of biexciton (solid symbols) and triexciton (open symbols) Auger lifetimes for CdSe NCs from this work (diamonds), Ref. 4 (circles), Ref. 25 (triangles), and Ref. 26 (squares). Lines are fits to a power dependence $\tau_{2,3} \propto R^m$. (b) The size dependence of the τ_2/τ_3 ratio for CdSe [solid diamonds (this work), open circles (Ref. 4), and solid triangles (Ref. 25)] and PbSe (squares) NCs in comparison to ratios expected for quadratic (2.25), cubic (3.375), statistical (4.5), and quantum-mechanical (2.5) scalings.

times that corresponds to different scalings is not very significant: It is ~40% if one compares quadratic and cubic scalings and ~30% for cubic and statistical τ_N dependences. The distinction, however, becomes more pronounced for multiexcitons of higher order. Specifically, the lifetimes that correspond to quadratic scaling quickly diverge from those calculated for cubic and statistical scalings with increasing N. On the other hand, even in the case of high-order multiexcitons, it is still difficult to make a distinction between cubic and statistical scalings. For example, for $N=5$, "quadratic" and "cubic" time constants differ by more than a factor of 2, while the corresponding difference for cubic and statistical scalings is still only ~40%. This indicates that given existing uncertainties in time-resolved measurements, differentiation between cubic and statistical scalings may

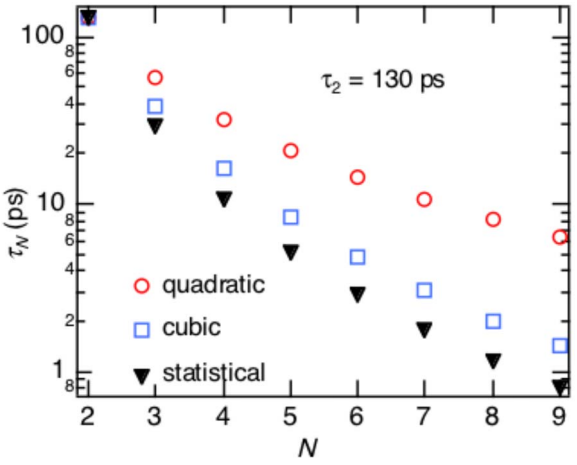

FIG. 4. (Color online) Calculated multiexciton Auger lifetimes for quadratic (open circles), cubic (open squares), and statistical (solid triangles) scalings of the τ_N time constants assuming a biexciton lifetime of 130 ps.

represent a significant experimental challenge, while it is less challenging to distinguish, for example, quadratic from cubic dependences of τ_N constants.

One approach to experimentally deriving lifetimes of high-order multiexcitons is through the subtractive procedure.[4] However, its accuracy quickly drops with increasing N. Therefore, in order to analyze relaxation behaviors of NC ensembles with large average occupancies, we perform numerical modeling of measured TA dynamics as outlined in the next section.

B. Modeling of transient absorption dynamics

In Fig. 5(a), we show TA dynamics measured at the position of the lowest-energy $1S$ absorption feature for CdSe NCs with $R=2.8$ nm for pump fluences that correspond to average initial occupancies $\langle N_0 \rangle$ from 0.56 to 5.4; $\langle N_0 \rangle$ is determined by the number of photons absorbed on average per NC, $\langle N_{ph,0} \rangle$, and can be calculated from $\langle N_0 \rangle = \langle N_{ph,0} \rangle = j_p \sigma$, where j_p is the per-pulse pump fluence (measured in photons/cm^2) and σ is the absorption cross section at the excitation wavelength.[23] The TA signals in CdSe NCs in the range of visible wavelengths are primarily due to three effects: state filling, Coulomb carrier-carrier interactions, and PA associated with charges trapped at NC interfaces.[23,29] On time scales longer than intraband relaxation times, the $1S$ bleach ($\Delta\alpha_{1S}$) is dominated by state filling. The corresponding contribution to $\Delta\alpha_{1S}$ is directly proportional to the occupation number of the $1S$ electron level and in the case of the Poisson distribution of occupation probabilities (expected at short times after photoexcitation before significant carrier recombination losses occur) it can be presented as[23,29]

$$\frac{|\Delta\alpha_{1S}|}{\alpha_{0,1S}} = \frac{1}{2}p_1 + \sum_{i=2}^{\infty} p_i = 1 - p_0 - \frac{1}{2}p_1 = 1 - \left(1 + \frac{\langle N \rangle}{2}\right)e^{-\langle N \rangle}, \tag{3}$$

where $\alpha_{0,1S}$ is the linear absorption at the position of the $1S$ resonance. The contribution of holes to $\Delta\alpha_{1S}$ is insignificant

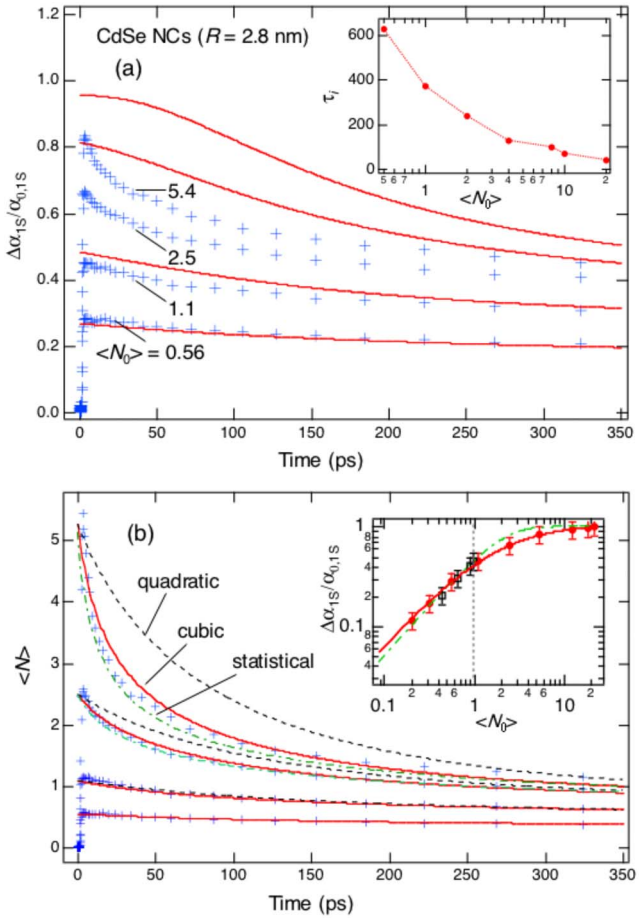

FIG. 5. (Color online) (a) 1*S* bleach dynamics measured for CdSe NCs with R=2.8 nm (symbols) for different pump fluences (100 fs, 3 eV pulses) that correspond to $\langle N_0\rangle$=0.56, 1.1, 2.5, and 5.4 (increasing from bottom to top); lines are calculations assuming the state-filling model and cubic scaling of τ_N (τ_2=130 ps). Obvious disagreement between the calculated and the measured traces indicates a significant influence of non-state-filling-related mechanisms on the 1*S* bleach dynamics. Inset: early-time instantaneous 1*S* bleach relaxation time (τ_i) as a function of initial average occupancy of the NCs. Steady decrease of τ_i with $\langle N_0\rangle$ in the range of pump fluences that correspond to $\langle N_0\rangle > 2$ indicates the sensitivity of the 1*S* bleach relaxation to recombination dynamics of multiexcitons with order greater than 2; this further confirms the importance of non-state-filling-related contributions to the 1*S* signal. (b) Pump-intensity-dependent dynamics of NC average occupancies extracted from TA traces in pl (a) using the phenomenological dependence of $\Delta\alpha_{1S}/\alpha_{0,1S}$ on $\langle N\rangle$ given in Eq. (4) with k_1=1.1 and k_2=1.6. The latter is shown by the solid line in the inset together with the experimental data points (solid circles; t=2 ps) and the dependence obtained for state filling alone assuming a Poisson distribution of carrier populations (dashed-dotted line). In the same plot, we also show the dependence of the measured long-term values of $\Delta\alpha_{1S}/\alpha_{0,1S}$ (t=325 ps) as a function of $\langle N\rangle$ (open squares); see text for details. Solid lines in the main frame are calculations for the cubic scaling; traces calculated for quadratic and statistical scalings are shown by the dashed and the dashed-dotted lines, respectively.

because the valence-band state involved in the absorbing transition stays unoccupied until the lower-energy emitting hole state is completely filled, which only occurs at high excitation levels. The role of holes in bleaching the 1*S* transition is further reduced because of a high spectral density of valence-band states, which leads to spreading of hole populations across many adjacent states not all of which are optically coupled to the 1*S* electron level.[30]

As illustrated in the inset of Fig. 5(b) [compare circles (experiment) and dashed-dotted line (state filling)], Eq. (3) describes an overall trend in the development of the 1*S* bleach with increasing pump level (measured 2 ps after excitation) reasonably well. The experimental data, however, show a systematic deviation from the state-filling model at high intensities. This deviation is due to contributions from Coulomb interactions and interface-related PA.[24,29] In order to account for these effects and more accurately describe the evolution of the 1*S* bleach with pump intensity, one can use the following phenomenological expression:

$$\frac{|\Delta\alpha_{1S}|}{\alpha_{0,1S}} = \frac{k_1\langle N\rangle}{k_2+\langle N\rangle} \tag{4}$$

proposed in Ref. 4; the coefficients k_1 and k_2 are sample dependent and are derived by fitting experimental pump dependences. In the case of the sample in the inset of Fig. 5(b), k_1=1.1 and k_2=1.6; these values are close to the parameters used in Ref. 4.

While having only a relatively small effect on saturation curves, the contribution from non-state-filling-related processes to the 1*S* TA signal greatly affects the measured dynamics. Specifically, within the state-filling model, the 1*S*-bleach decay in CdSe NCs is governed by recombination of singly and doubly excited NCs, which is a consequence of the twofold degeneracy of the 1*S* electron level. However, measured transients indicate a steady decrease of the instantaneous decay constant, τ_i, for $\langle N\rangle$ greatly exceeding 2 [main panel and inset of Fig. 5(a)]. For example, we measure τ_i =40 ps for $\langle N\rangle$=20, which is much shorter than the biexciton lifetime for this sample (τ_2=130 ps). This result shows that the 1*S* bleach decay can be used to infer lifetimes of NC states with multiplicity greater than 2.

In order to translate measured TA dynamics into dynamics of the NC average occupancy, $\langle N(t)\rangle$, we use Eq. (4), which is the approach applied previously in Ref. 4. The dependence described in Eq. (4) was derived on the basis of early-time TA values; therefore, it is not obvious that it is applicable at arbitrary times after excitation. On the other hand, one can easily see that it provides an accurate description of the relationship between $\Delta\alpha_{1S}(t)$ and $\langle N(t)\rangle$ at long times after excitation ($t \gg \tau_2$) when all multiexcitons have decayed to produce single excitons, and hence, $\langle N\rangle$ is smaller than 1. In this case, the NC average occupancy is equal to the number of initially excited NCs (we assume that t is shorter than the single-exciton lifetime) and can be calculated from $\langle N\rangle|_{\tau_2 \ll t \ll \tau_1} = 1 - p_0 = 1 - \exp(-\langle N_0\rangle)$. The plot of the long-time values of $\Delta\alpha_{1S}/\alpha_{0,1S}$ as a function $\langle N\rangle$ [open squares in the

inset of Fig. 5(b)] closely follows the dependence given in Eq. (4). The fact that this dependence describes well the experimental data in the limit of both short and long times after excitation allows us to assume that it also is applicable on the intermediate time scales.

The $\langle N(t)\rangle$ dynamics extracted from TA traces in Fig. 5(a) are displayed in panel (b) of the same figure (symbols). To model these dynamics, we use coupled rate equations for probabilities $p_i(t)$ given by Eq. (1). To calculate the initial probabilities $[p_i(t=0)=p_i(0)]$, we assume a Poisson distribution of NC populations, for which $p_i(0)=(\langle N_0\rangle^i/i!)\exp(-\langle N_0\rangle)$. After numerically solving the rate equations, we calculate the population dynamics $\langle N(t)\rangle=\sum_{i=0}^{\infty} i p_i(t)$, and then, compare them with dynamics derived from the measured TA traces.

We find solutions of Eq. (1) for quadratic, cubic, and statistical scalings of the τ_N time constants [dashed, solid, and dashed-dotted lines in Fig. 5(b), respectively]. In the case of the sample with $R=2.8$ nm, quadratic scaling results in dynamics that clearly disagree with experimental traces. The dynamics calculated for the cubic and statistical scalings do not significantly differ from each other, and both are in reasonable agreement with the experimental data. However, the fact that the measured τ_2/τ_3 ratio for this sample is more consistent with the cubic scaling suggests that the $\tau_N \propto N^{-3}$ dependence is best suited for describing multiexciton dynamics in this case.

Using $\langle N(t)\rangle$ dynamics computed for cubic scaling, we also calculate TA dynamics by taking into account only the state-filling contribution to the $1S$ bleach. The results of these calculations are shown by lines in Fig. 5(a) in comparison to measured traces (symbols). We observe that at low and moderate pump intensities ($\langle N_0\rangle=0.56$ and 1.1), the state-filling model provides a reasonable agreement with experimental time transients. On the other hand, this model clearly disagrees with the experiment at high intensities ($\langle N_0\rangle>2$), which highlights the importance of non-state-filling induced contributions to band-edge TA signals; because of these contributions, higher-order multiexcitons have a significant effect on the $1S$ bleach relaxation dynamics.

We have also modeled TA dynamics for smaller NCs with $R=1.7$ nm (Fig. 6). In this case, the $1S$ bleach measured at 2 ps after excitation initially shows saturation with increasing pump intensities (as expected from state-filling arguments), but then it starts to decrease (at $\langle N_0\rangle>3$), as a result of PA associated with surface-trapped charges (left inset of Fig. 6).[24] As was observed previously,[24] the contribution from PA, which grows almost linearly with $\langle N_0\rangle$, can eventually completely suppress bleaching, which results in the situation when the $1S$ signal is dominated by induced absorption. The effect of PA leads to a nonmonotonic dependence of $\Delta\alpha_{1S}$ on pump fluence, which complicates the extraction of $\langle N(t)\rangle$ dynamics from the TA traces measured at high pump intensities. Therefore, in our modeling, we limit our analysis to time transients recorded for $\langle N_0\rangle<3$ (Fig. 6, main frame).

For initial occupancies studied here, quadratic, cubic, and statistical scalings produce similar relaxation dynamics (shown in Fig. 6 by solid, dashed, and dashed-dotted lines, respectively), all of which are in reasonable agreement with the experiment [compare different-style lines (modeling) with symbols (experiment) for $\langle N_0\rangle=2.2$]. The inspection of short-term dynamics (right inset of Fig. 6), however, indicates that the N^2 dependence of τ_N^{-1} may provide a slightly better description of experimental data compared to the two other scaling laws. In combination with the measured τ_2/τ_3 ratios for NCs of small sizes [Fig. 3(b)], this points toward the quadratic scaling in small CdSe NCs.

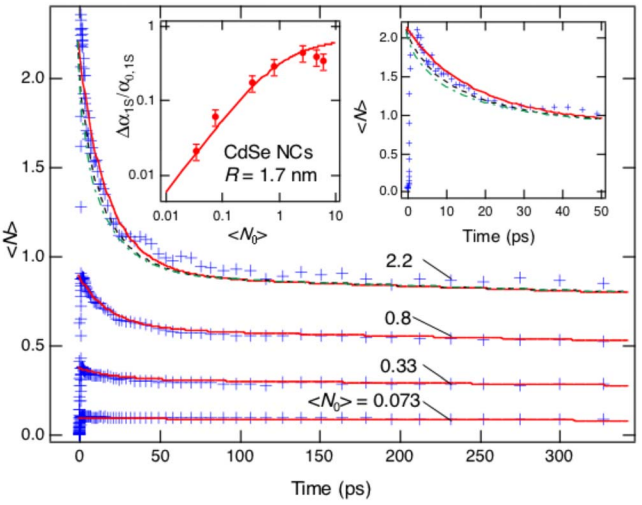

FIG. 6. (Color online) (a) NC average population dynamics extracted from $1S$ bleach time transients measured for CdSe NCs with $R=1.7$ nm (symbols) for different pump fluences (100 fs, 3 eV pulses) that correspond to $\langle N_0\rangle=0.073$, 3.3, 0.8, and 2.2. Solid lines are calculations assuming quadratic scaling of τ_N ($\tau_2=20$ ps); the transient measured for $\langle N_0\rangle=2.2$ is also compared to calculations for cubic (dashed line) and statistical (dashed-dotted line) scalings. The inset on the right is the expanded view of early-time dynamics measured for $\langle N_0\rangle=2.2$ in comparison to calculations (line styles are the same as in the main frame). The inset on the left is the pump-intensity dependence of the $1S$ bleach (symbols) in comparison to a fit using the phenomenological dependence given in Eq. (4) with $k_1=0.67$ and $k_2=1.13$ (line).

Thus, the analysis of a large body of experimental data for biexciton and triexciton lifetimes in CdSe NCs indicates that the ratio of the τ_2 and τ_3 time constants is smaller than that expected for statistical scaling. The observed size dependence of this ratio (τ_2/τ_3 increases from ~2.3 to ~3.4 for R increasing from 1.45 to 4.2 nm) as well as the absolute τ_2/τ_3 values can be interpreted in terms of size-dependent scaling that changes from approximately quadratic at small NC sizes to cubic at large sizes; numerical modeling using this size-dependent scaling allows us to describe the measured TA dynamics reasonably well. As suggested by our quantum-mechanical modeling (Sec. III), the observed deviation from statistical scaling likely results from the "asymmetric" character of high-order multiexcitons ($N>2$) that in CdSe NCs necessarily comprise both S and non-S-type carriers These asymmetric multiexcitons are characterized by reduced rates of Auger decay compared to symmetric multiexcitons because of a reduced number of recombination pathways.

V. MULTIEXCITON DYNAMICS IN LEAD SELENIDE NANOCRYSTALS

A. High-intensity excitation

In the present work, we have also experimentally studied the regime of highly degenerate $1S$ states using PbSe NCs. A multivalley character of a band structure of lead chalcogenides (four equivalent band minima at the L points of the Brillouin zone) together with a twofold spin degeneracy lead to the high, eightfold total degeneracy of the electron and the hole $1S$ levels in PbSe NCs.[13,31] In this case, one can expect to observe statistical scaling of τ_N up to $N=8$. Further, because of this high degeneracy, the $1S$ bleach ($\Delta\alpha_{1S}$) is nearly linear in $\langle N\rangle$ for NC average occupancies up to ~ 5;[13] therefore, $\Delta\alpha_{1S}$ (monitored using a TA experiment) provides an accurate measure of $\langle N\rangle$ even in the case of high-order multiexcitons. This situation is more favorable compared to that in CdSe NCs, where the $1S$ bleach rapidly saturates for $\langle N\rangle > 1$.

First, as in the case of CdSe NCs, we use a subtractive procedure[4] to extract biexciton and triexciton dynamics from pump-intensity-dependent TA traces such as those in Fig. 7(a) ($R=4$ nm, $T=300$ K). An example of such dynamics (in comparison to single-exciton decay) is shown in the inset of Fig. 7(a). Using these data ($\tau_2=160$ ps, $\tau_3=40$ ps), we obtain $\tau_2/\tau_3=4$. For NCs of smaller radius ($R=2$ nm), we measure $\tau_2=50$ ps and $\tau_3=16$ ps, which yields $\tau_2/\tau_3=3.1$. For both sizes, the measured ratios are greater than the quadratic value (2.25) and are rather indicative of scaling that is at least cubic.

Following this initial analysis of τ_N scaling based of the τ_2/τ_3 values, we proceed to numerical modeling of $1S$ TA dynamics using coupled "Auger" rate equations, as described in Sec. IV B. We again consider three different scaling laws: quadratic, cubic, and statistical. In our previous studies of PbSe NCs, in the regime when multiexcitons were generated via CM,[32] we utilized a quadratic scaling of τ_N^{-1} based on results of earlier studies of CdSe NCs.[4] However, modeling of TA data for NCs with $R=4$ nm [Fig. 7(b)] shows that the N^3 and $N^2(N-1)$ scalings provide a better description of the experimental data than the N^2 scaling. Further, a closer inspection of early time dynamics [inset of Fig. 7(b)] indicates that statistical scaling describes the experimental data slightly better than the cubic one. Using the $N^2(N-1)$ scaling and $\tau_2=160$ ps (derived by the subtractive procedure), we can accurately model all dynamics recorded for $\langle N\rangle$ from 0.36 to 5.1 without any fitting parameters or additional normalization [Fig. 7(a)].

We observe some discrepancy between calculated and measured dynamics at early times after excitation. This discrepancy is likely attributed to the fact that because of rapid shortening of Auger lifetime with N, the higher-order multiexciton decay times are comparable to or even shorter than the exciton cooling time. Specifically, given intraband energy loss rates measured in Ref. 33, it takes ~ 10 ps or longer for carriers to relax from the initially excited state produced by 1.5 eV photons to the band-edge $1S$ levels. The latter value is longer than the Auger lifetime of, e.g., the five-exciton state, which is ~ 6 ps (estimated for $\tau_2=160$ ps and statistical scaling of τ_N). In this situation, multiexcitons with $N>4$ do not appreciably contribute to the $1S$ bleach, which can explain the fact that the amplitude of the measured TA traces is decreased compared to the amplitude of the calculated transients.

Because of the competition between Auger decay and intraband relaxation (exciton cooling), rapid shortening of Auger lifetimes with decreasing R ($\tau_N \propto R^3$; Ref. 4) leads to decreasing contribution from higher-order multiexcitons to the $1S$ bleach in smaller NCs, which makes it more difficult to infer the scaling of τ_N from experimental data. For example, our modeling of experimental dynamics for NCs with $R=2$ nm [Fig. 7(c); main panel and inset] indicates that both the statistical and cubic scalings of τ_N^{-1} describe TA traces better than the quadratic scaling. However, it is difficult to further distinguish between the N^3 and $N^2(N-1)$ scalings, because rapid Auger decay of high-order multiexcitons during intraband relaxation effectively limits the average NC occupancy probed in the TA experiment.

B. Multiexciton generation via carrier multiplication

A clearer distinction between different scaling laws for τ_N can, in principle, be made using the CM regime for generating multiexcitons.[8] In this process, multiple e-h pairs are produced at low pump intensities by single photons. High-efficiency CM was first observed in PbSe NCs,[8] and then, in a number of other NCs using both spectroscopic[27,34–38] and photocurrent measurements.[39] The exact mechanism for CM in NCs is still under debate. The proposed models include traditional impact ionization,[40–42] coherent evolution of the initially excited single-exciton state,[43] direct photoexcitation of biexcitons via intermediate single-exciton states,[44] and photostimulated generation of biexcitons from vacuum mediated by intraband optical transitions.[45]

In the case when multiexcitons are produced by CM, the average per-exciton excess energy (ΔE_x) is approximately determined by the expression $\Delta E_x=(\hbar\omega-E_g)/\langle N_x\rangle$, where $\langle N_x\rangle \geqslant 1$ is the average exciton multiplicity (the number of excitons per photoexcited NC); this quantity is also used as a measure of the CM efficiency. The latter expression indicates that in the CM case, when $\langle N_x\rangle > 1$, the per-exciton excess energy is smaller than that in the regime of traditional high-intensity excitation [$\Delta E_x=(\hbar\omega-E_g)$], which should result in reduced exciton cooling times. The shortening of the carrier cooling time in the CM excitation regime compared to the no-CM case was experimentally observed in Ref. 44. This effect is useful for the purpose of the present study because it reduces carrier losses associated with Auger decay during the initial stage of intraband relaxation, and hence, can allow probing states of higher exciton multiplicity. Another property of the CM process, useful in studies of multiexcitons, is that it produces a narrow, non-Poissonian distribution of exciton multiplicities (potentially, a single-multiplicity ensemble state),[32] for which initial ensemble dynamics are governed by recombination of just one or two high-order multiexcitons.

In modeling the decay of the multiexciton system produced by CM, one needs to account for the fact that in this

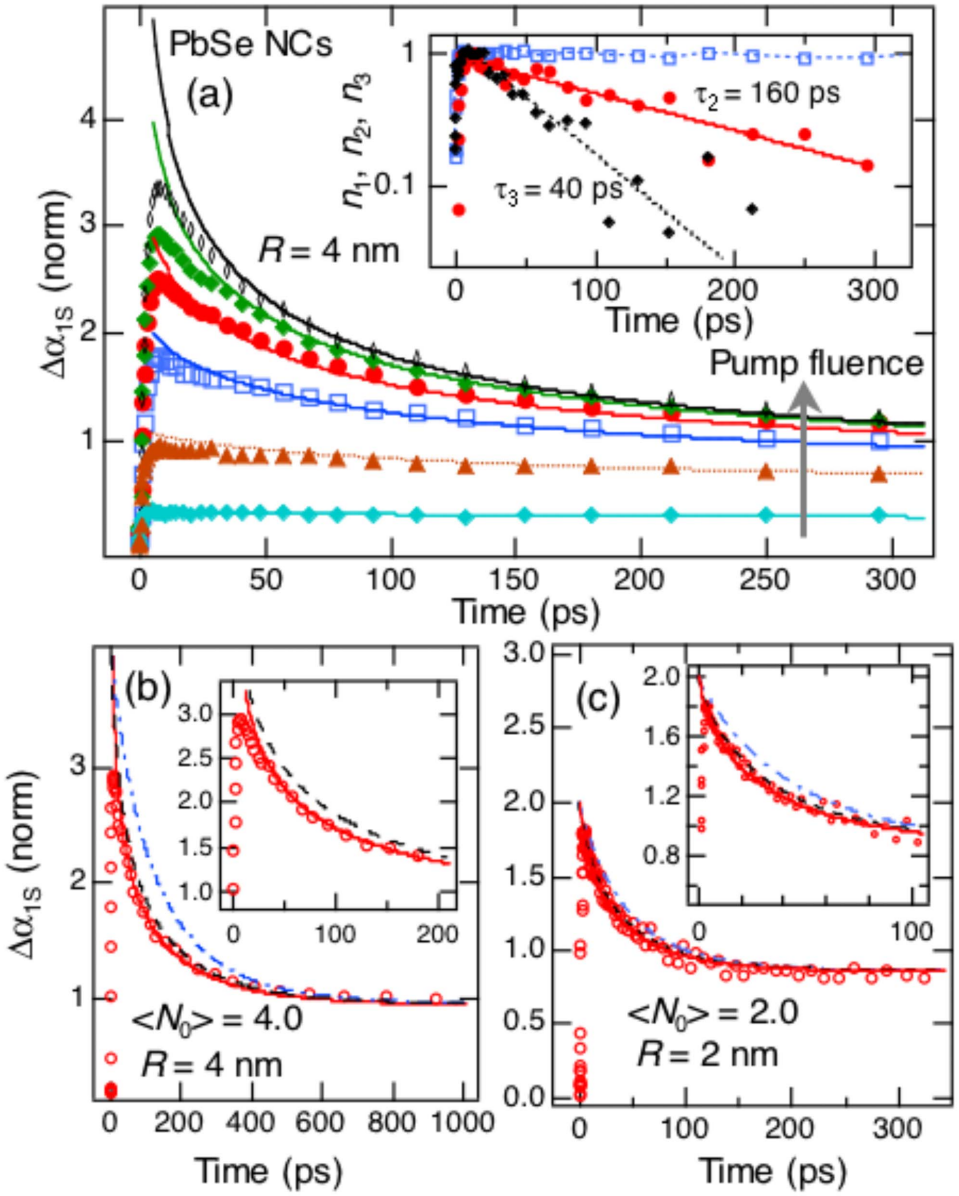

FIG. 7. (Color online) (a) 1*S* bleach dynamics measured for PbSe NCs with $R=4$ nm (symbols) for different pump fluences (50 fs, 1.5 eV pulses) that correspond to $\langle N_0\rangle=\langle N(t=0)\rangle=0.35$, 1.1, 2, 2.9, 4, and 5.1 (increasing from bottom to top); lines are calculations assuming statistical scaling of τ_N ($\tau_2=160$ ps). Inset: biexciton (circles) and triexciton (diamonds) dynamics extracted from TA traces in comparison to single-exciton dynamics (squares). [(b) and (c)] 1*S* bleach dynamics for PbSe NCs with $R=4$ nm and 2 nm (initial average NC occupancies are 4 and 2, respectively) modeled assuming statistical (solid line), cubic (dashed line), or quadratic (dashed-dotted line) scalings of τ_N. The inset in pl (b) is the expanded view of early-time dynamics, which indicates that in the case of the 4 nm sample, statistical scaling provides a better fit of experimental data than cubic scaling. The expanded view of early-time dynamics for the 2 nm sample [inset in pl (c)] shows that both cubic and statistical scalings describe experimental data better than the quadratic one. On the other hand, based on these data it is difficult to further distinguish between the statistical and the cubic scalings.

case, the distribution of initial ($t=0$) NC occupancies is different compared to the no-CM situation when multiple e-h pairs are produced via absorption of multiple photons from the same pump pulse. As was pointed out in the previous subsection, in the latter case, the initial NC occupancies can be accurately described by Poisson statistics, for which the average ensemble multiplicity is directly linked to average occupancy ($\langle N_{x0}\rangle=\langle N_0\rangle(1-e^{-\langle N_0\rangle})^{-1}$),[32] and hence per-pulse pump fluence. In the CM regime (low excitation intensities, for which $\langle N_{ph,0}\rangle \ll 1$), initial occupancies are non-Poissonian and the average ensemble multiplicity is determined not by the pump fluence but by the pump-photon energy.[32] Specifically, in this case, the photoexcited NC ensemble is characterized by two dominant multiplicities $m=\lfloor 1.14\eta\omega/E_g-2.25\rfloor$ and $l=m+1$ ("$\lfloor X\rfloor$" is the rounded-down value of X). The respective fractions of photoexcited NCs are

$$f_m = m - 1.14(\hbar\omega/E_g - 2.85) \quad \text{and} \quad f_l = 1 - f_m, \tag{5}$$

while the corresponding probabilities calculated taking into account both excited and unexcited NCs are $p_{m(l)}|_{t=0}$

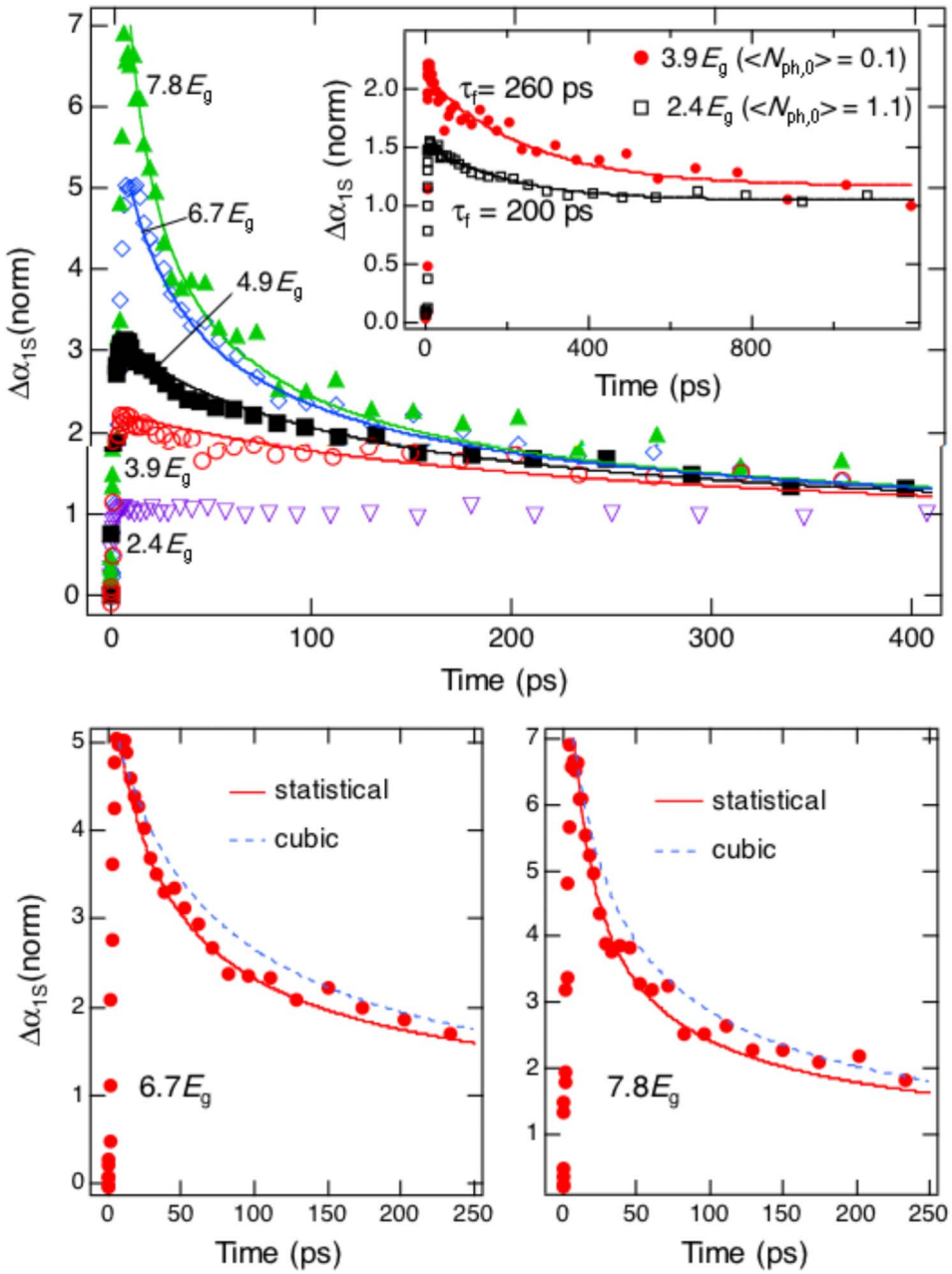

FIG. 8. (Color online) (a) 1*S* bleach dynamics for PbSe NCs with R=4.2 nm (symbols) measured at low pump intensity ($\langle N_{ph,0}\rangle$=0.1) and different photon energies from 2.4 to 7.8E_g (indicated in the figure). These measured traces are modeled (lines) using initial average multiplicities 1, 2.2, 3, 5, and 7 (from bottom to top) and assuming statistical scaling of τ_N time constants. The biexciton lifetime is derived from a single-exponential fit of the initial fast TA decay (τ_f=260 ps) measured with 3.9E_g photons ($\langle N_{ph,0}\rangle$=0.1), for which CM is expected to primarily produce biexcitons (inset; solid circles); the fit of the TA trace measured using high-intensity ($\langle N_{ph,0}\rangle$=1.1), low-photon-energy (2.4E_g) excitation produces a fast decay component with a time constant of 200 ps (inset; open squares). [(b) and (c)] 1*S* TA dynamics (symbols) measured with 6.7E_g and 7.8E_g photons modeled using either cubic (dashed line) or statistical (solid line) scaling of Auger lifetimes.

$=f_{m(l)}\langle N_{ph,0}\rangle$ (for m, $l>0$) and $p_0|_{t=0}=1-\langle N_{ph,0}\rangle$.

In Fig. 8(a), we show TA dynamics recorded at low pump intensity ($\langle N_{ph,0}\rangle$=0.1) for photon energies from 2.4 to 7.8E_g for a sample with an NC size that is close to that in Fig. 7. These traces are normalized to the height of the slow, single-exciton background. In this representation, the TA values represent a direct measure of average multiplicity $\langle N_x\rangle$,[8,32,44] which can be related to probabilities p_i by $\langle N_x\rangle = (1/\langle N_{ph,0}\rangle)\Sigma_{i=1}^{\infty} ip_i = \Sigma_{i=1}^{\infty} if_i$.[32] We use this expression to model TA transients in Fig. 8. We calculate probabilities p_i by solving a set of coupled Auger equations [Eq. (1)]. The initial values of p_i are found from Eq. (5) on the basis of experimental pump-photon energies. We further consider either statistical or cubic scaling of τ_N time constants with τ_2 =260 ps, as derived from a single-exponential fit to dynamics measured for $\hbar\omega$=3.9E_g [inset of Fig. 8(a)], when CM

primarily produces biexcitons. The latter time constant is close to that [~200 ps; inset of Fig. 8(a)] measured using low-photon-energy, high-intensity excitation (no CM).

We see that in the CM case, the distinction between the statistical and cubic scalings is more pronounced than in the no-CM situation [Figs. 8(b) and 8(c)], which is because of both higher initial exciton multiplicity and smaller number multiplicities contributing to early-time dynamics. The comparison of calculated and measured TA traces indicates that statistical scaling reproduces the measured dynamics more closely than the cubic one. Furthermore, using statistical scaling, we can model all of the dynamics in the main panel of Fig. 8(a) without any adjustable parameters by using initial multiplicities ($\langle N_{x0}\rangle$ from 1 to ~7) derived from experimental pump-photon energies.

Thus, in PbSe NCs, the measured τ_2/τ_3 ratios are larger than those in CdSe NCs and indicate that the τ_N scaling is faster than quadratic. For the large-size sample ($R=4$ nm), the TA dynamics measured using both traditional (high pump intensity) and CM excitation regimes can be accurately modeled using statistical scaling of multiexciton time constants. This scaling also describes the dynamics measured for the smaller-size sample ($R=2$ nm) well. However, in the latter case, we cannot exclude the possibility of the cubic scaling, because for initial exciton multiplicities accessible in our experiments, the dynamics calculated for the cubic and statistical scalings are very similar to each other.

VI. CONCLUSIONS

In conclusion, we have experimentally and theoretically studied multiexciton dynamics in semiconductor NCs with a goal to infer the scaling of Auger decay constants with the number of excitons per NC, N. We showed that in determining this scaling, it is important to distinguish between ensemble-averaged ($\tau^*_{\langle N\rangle}$) and single-NC ($\tau_N$) multiexciton lifetimes. In the large-N limit, $(\tau^*_{\langle N\rangle})^{-1}$ scales quadratically with $\langle N\rangle$, which is similar to the quadratic scaling of instantaneous Auger decay rates with carrier density in the bulk. In the same limit ($N\gg 1$), the single-NC multiexciton decay constants scale cubically with N: $\tau_N^{-1}\propto BN^3$.

We further analyze theoretically the τ_N scaling for the situation of a small number of excitons per NC using first-order perturbation theory. This analysis indicates that in the case of multiexcitons built from states of identical symmetry (symmetric multiexcitons), one may expect the statistical scaling of Auger lifetimes, $\tau_N^{-1}\propto N^2(N-1)$, as determined by the total number of individual Auger transitions. On the other hand, the τ_N scaling is expected to deviate from statistical for asymmetric multiexcitons (built, e.g., from both $1S$ and $1P$ states) because of reduced probability of recombination between electron and hole states of different symmetries. Specifically, the "quantum-mechanical" ratio of the τ_2 and τ_3 lifetimes calculated neglecting S-P recombination (2.5) is close to that for quadratic scaling (2.25). The deviation from the statistical scaling can also result from geometrical constraints existing, for example, in 1D systems.

To experimentally realize situations of symmetric and asymmetric multiexcitons, we studied, respectively, PbSe and CdSe NCs. In PbSe nanoparticles, the $1S$ conduction- and valence-band levels can accommodate up to eight carriers; therefore, multiexcitons with order up to 8 can be built from the same $1S$-type wave functions. On the other hand, the $1S$ electron state in CdSe NCs is twofold degenerate; therefore, multiexcitons of order $N>2$ necessarily involve both S and non-S symmetry states. We experimentally determined the τ_N scaling from the measured ratio of the τ_2 and τ_3 time constants and also from modeling of TA dynamics using three different scaling laws: statistical, cubic, and quadratic. In the case of CdSe NCs, the measured τ_2/τ_3 ratio can be interpreted in terms of size-dependent scaling, which changes from approximately quadratic to cubic with increasing R. On the basis of our theoretical studies, we can attribute this deviation from statistical scaling to the reduced probability of Auger transitions involving e-h recombination between states of S and P symmetries.

The τ_2/τ_3 ratios measured for PbSe NCs are larger than those for CdSe NCs and indicate that for studied sizes the τ_N scaling is at least cubic. To further distinguish between cubic and statistical scalings, we analyzed TA dynamics using a set of coupled Auger equations. For larger NCs ($R=4$ nm), we studied two excitation regimes with multiexcitons produced either by high-intensity pulses via absorption of multiple photons or by single high-energy photons using the CM process. The latter regime allows a clearer distinction between different scaling laws for τ_N because it results in higher exciton multiplicities and a narrower, non-Poissonian distribution of initial multiplicities. Numerical modeling based on coupled Auger equations indicates that the measured TA dynamics for both excitation regimes can be best described by statistical scaling. On the other hand, in the case of smaller NCs ($R=2$ nm), based on modeling of Auger equations, we cannot make a conclusive distinction between statistical and cubic scalings because they produce very similar relaxation dynamics for initial multiplicities realized under our experimental conditions. The differentiation between these two scalings, in general, represents a challenging experimental task because the corresponding constants are not significantly different even in the case of high-order multiexcitons with $N>3$.

ACKNOWLEDGMENTS

This work was supported by the Chemical Sciences, Biosciences, and Geosciences Division of the Office of Basic Energy Sciences, Office of Science, U.S. Department of Energy (DOE) and Los Alamos LDRD funds. V.I.K. acknowledges partial support by the DOE Center for Integrated Nanotechnologies jointly operated by Los Alamos and Sandia National Laboratories.

[1] M. Nirmal, D. J. Norris, M. Kuno, M. G. Bawendi, A. L. Efros, and M. Rosen, Phys. Rev. Lett. **75**, 3728 (1995).
[2] A. L. Efros, V. A. Kharchenko, and M. Rosen, Solid State Commun. **93**, 281 (1995).
[3] V. I. Klimov and D. W. McBranch, Phys. Rev. Lett. **80**, 4028 (1998).
[4] V. I. Klimov, A. A. Mikhailovsky, D. W. McBranch, C. A. Leatherdale, and M. G. Bawendi, Science **287**, 1011 (2000).
[5] V. I. Klimov and D. W. McBranch, Phys. Rev. B **55**, 13173 (1997).
[6] V. I. Klimov, A. A. Mikhailovsky, S. Xu, A. Malko, J. A. Hollingsworth, C. A. Leatherdale, H. J. Eisler, and M. G. Bawendi, Science **290**, 314 (2000).
[7] V. I. Klimov, S. A. Ivanov, J. Nanda, M. Achermann, I. Bezel, J. A. McGuire, and A. Piryatinski, Nature (London) **447**, 441 (2007).
[8] R. D. Schaller and V. I. Klimov, Phys. Rev. Lett. **92**, 186601 (2004).
[9] A. J. Nozik, Physica E (Amsterdam) **14**, 115 (2002).
[10] P. T. Landsberg, *Recombination in Semiconductors* (Cambridge University Press, Cambridge, 1991).
[11] D. I. Chepic, A. L. Efros, A. I. Ekimov, M. G. Ivanov, V. A. Kharchenko, and I. A. Kudriavtsev, J. Lumin. **47**, 113 (1990).
[12] L.-W. Wang, M. Califano, A. Zunger, and A. Franceschetti, Phys. Rev. Lett. **91**, 056404 (2003).
[13] R. D. Schaller, M. A. Petruska, and V. I. Klimov, J. Phys. Chem. B **107**, 13765 (2003).
[14] S. A. Crooker, T. Barrick, J. A. Hollingsworth, and V. I. Klimov, Appl. Phys. Lett. **82**, 2793 (2003).
[15] B. L. Wehrenberg, C. J. Wang, and P. Guyot-Sionnest, J. Phys. Chem. B **106**, 10634 (2002).
[16] R. D. Schaller, M. Sykora, J. M. Pietryga, and V. I. Klimov, Nano Lett. **6**, 424 (2006).
[17] P. C. Findlay, C. P. Pidgeon, R. Kotitschke, A. Hollingworth, B. N. Murdin, C. J. G. M. Langerak, A. F. G. van der Meer, C. M. Ciesla, J. Oswald, A. Homer, G. Springholz, and G. Bauer, Phys. Rev. B **58**, 12908 (1998).
[18] H. Zogg, W. Vogt, and W. Baumgartner, Solid-State Electron. **25**, 1147 (1982).
[19] A. A. Abrikosov, L. P. Gorkov, and I. E. Dzyaloshinskii, *Methods of Quantum Field Theory in Statistical Physics* (Dover, New York, 1975).
[20] T. Uozumi, Y. Kayanuma, K. Yamanaka, K. Edamatsu, and T. Itoh, Phys. Rev. B **59**, 9826 (1999).
[21] H. Htoon, J. A. Hollingsworth, R. Dickerson, and V. I. Klimov, Phys. Rev. Lett. **91**, 227401 (2003).
[22] L. Huang and T. D. Krauss, Phys. Rev. Lett. **96**, 057407 (2006).
[23] V. I. Klimov, J. Phys. Chem. B **104**, 6112 (2000).
[24] A. V. Malko, A. A. Mikhailovsky, M. A. Petruska, J. A. Hollingsworth, and V. I. Klimov, J. Phys. Chem. B **108**, 5250 (2004).
[25] B. Fisher, J.-M. Caruge, Y.-T. Chan, J. Halpert, and M. G. Bawendi, Chem. Phys. **318**, 71 (2005).
[26] M. Achermann, J. A. Hollingsworth, and V. I. Klimov, Phys. Rev. B **68**, 245302 (2003).
[27] R. D. Schaller, J. M. Pietryga, and V. I. Klimov, Nano Lett. **7**, 3469 (2007).
[28] A. Pandey and P. Guyot-Sionnest, J. Chem. Phys. **127**, 111104 (2007).
[29] V. I. Klimov, Annu. Rev. Phys. Chem. **58**, 635 (2007).
[30] V. I. Klimov, D. W. McBranch, C. A. Leatherdale, and M. G. Bawendi, Phys. Rev. B **60**, 13740 (1999).
[31] I. Kang and F. W. Wise, J. Opt. Soc. Am. B **14**, 1632 (1997).
[32] R. D. Schaller and V. I. Klimov, Phys. Rev. Lett. **96**, 097402 (2006).
[33] R. D. Schaller, J. M. Pietryga, S. V. Goupalov, M. A. Petruska, S. A. Ivanov, and V. I. Klimov, Phys. Rev. Lett. **95**, 196401 (2005).
[34] R. Ellingson, M. C. Beard, J. C. Johnson, P. Yu, O. I. Micic, A. J. Nozik, A. Shabaev, and A. L. Efros, Nano Lett. **5**, 865 (2005).
[35] J. Murphy, M. Beard, A. Norman, S. Ahrenkiel, J. Johnson, P. Yu, O. Micic, R. Ellingson, and A. Nozik, J. Am. Chem. Soc. **128**, 3241 (2006).
[36] M. C. Beard, K. P. Knutsen, P. Yu, J. M. Luther, Q. Song, W. K. Metzger, R. J. Ellingson, and A. J. Nozik, Nano Lett. **7**, 2506 (2007).
[37] R. D. Schaller, M. A. Petruska, and V. I. Klimov, Appl. Phys. Lett. **87**, 253102 (2005).
[38] D. Timmerman, I. Izeddin, P. Stallinga, I. N. Yassievich, and T. Gregorkiewicz, Nat. Photonics **2**, 105 (2008).
[39] S. J. Kim, W. J. Kim, Y. Sahoo, A. N. Cartwright, and P. N. Prasad, Appl. Phys. Lett. **92**, 031107 (2008).
[40] M. Califano, A. Zunger, and A. Franceschetti, Appl. Phys. Lett. **84**, 2409 (2004).
[41] M. Califano, A. Zunger, and A. Franceschetti, Nano Lett. **4**, 525 (2004).
[42] G. Allan and C. Delerue, Phys. Rev. B **73**, 205423 (2006).
[43] A. Shabaev, A. L. Efros, and A. J. Nozik, Nano Lett. **6**, 2856 (2006).
[44] R. D. Schaller, V. M. Agranovich, and V. I. Klimov, Nat. Phys. **1**, 189 (2005).
[45] V. I. Rupasov and V. I. Klimov, Phys. Rev. B **76**, 125321 (2007).